IEEE Access
Multidisciplinary | Rapid Review | Open Access Journal

Received December 6, 2019, accepted December 22, 2019, date of publication January 1, 2020, date of current version January 10, 2020.

Digital Object Identifier 10.1109/ACCESS.2019.2963097

Magnetic Viscosity Effect on Grounded-Wire TEM Responses and Its Physical Mechanism

LINBO ZHANG[1,2,3], HAI LI[1,2], (Member, IEEE), GUOQIANG XUE[1,2,3], WEN CHEN[1,2,3], AND YIMING HE[1,2,3]

[1]Key Laboratory of Mineral Resources, Institute of Geology and Geophysics, Chinese Academy of Sciences, Beijing 100029, China
[2]University of Chinese Academy of Sciences, Beijing 100049, China
[3]Innovation Academy for Earth Science, Chinese Academy of Sciences, Beijing 100029, China

Corresponding author: Hai Li (thinda@163.com)

This work was supported in part by the Beijing Natural Science Foundation under Grant 8184089, in part by the Natural Science Foundation of China under Grant 41804074, Grant 41874088, Grant 41752440, and Grant 41874162, and in part by the S&T Program of Beijing under Grant Z181100005718001.

ABSTRACT Magnetic viscosity (MV) effect is a disturbance to the transient electromagnetic method (TEM). This effect will cause slow decay at the intermediate-late time of the TEM responses, leading to erroneous interpretation. Although there are extensive researches on the MV distortion to TEM data, they are focused on conventional loop source configuration, while little has been studied for grounded-wire source configuration that has become the essential role for relatively deep-buried targets. Hence, we present the study of MV effect on the grounded-wire source TEM data. We first derived the formulas for calculating the secondary field due to MV effect, based on the Chikazumi model. The dependence of the MV effect on model parameters, such as resistivity, susceptibility, offset and geometry of the superparamagnetic layer, is then examined to illustrate the intrinsic physical mechanism of MV effect. We find that the MV effect on the grounded-wire source TEM data can be suppressed by adjusting the parameters of the survey design. Thereafter, we propose the method to quantify the MV effect when estimates of resistivity and susceptibility are available. Finally, the method for choosing the optimal offset to suppress the MV effect is proposed, which can be used as a guide for the installation of fieldwork of grounded-wire TEM survey.

INDEX TERMS Grounded-wire source TEM, magnetic viscosity effect, Chikazumi model, physical mechanism, superparamagnetic.

I. INTRODUCTION

Transient electromagnetic method (TEM) is an important tool to obtain the electric properties in near-surface detection. The method can be used in the scenarios of land, marine and airborne surveys [1]–[3], and has been widely used in mineral detection, engineering investigation and hydrocarbon exploration [4], [5]. The TEM method uses the grounded-wire or ungrounded-loop to transmit an electromagnetic signal to the earth and records the induced electromagnetic field after the source is switched off. The resistivity of the earth can be estimated from the recorded signal using inversion or imaging techniques.

When superparamagnetic (SPM) media are presented in the subsurface, the magnetic susceptibility will vary with time. The resulting magnetic viscosity (MV) effect generates a secondary electromagnetic field that merges together with the secondary field from electromagnetic induction. The attenuation rate of late time TEM response will be greatly reduced [6]. In some cases, the additional MV signal can be can be regard as a useful indicator of magnetic targets, such as the filed of archaeological prospecting, magnetic mineral investigation, and the detection of glacial till [7]–[11]. MV signal can also provide the quantitative magnetic information of survey area with the definition of time-dependent magnetic susceptibility [12]. However, in most cases, the MV effect acts as a disturbance to the TEM data. The inversion method for TEM data is incapable of handling the MV distorted responses. Therefore, the late time responses in this condition are commonly discarded, leading to the absence of information for the deep target [13], [14]. In addition, if the data are inverted without considering the MV effect, a spurious conductive anomaly may be obtained, which will lead to incorrect delineation of the targets [14], [15].

The associate editor coordinating the review of this manuscript and approving it for publication was Geng-Ming Jiang.

The MV effect in the TEM data is caused by the magnetite and hematite particles with a radius of 0.1-15 um, according to the results of petrophysical experiments [15]–[19]. Under a natural condition, the SPM medium originates from basalt, tuff, and magnetic minerals [20]. Driven by the weathering denudation, water erosion, ancient cultural activities and the enrichment of magnetotactic bacteria, the MV effect are widely distributed in the targets of TEM survey, such as magnetic metal resources (magnetite, hematite, nickel, etc.), UXO, and the targets in the permafrost, archaeology investigations [7], [9], [12], [21]–[23]. Therefore, the research of the mechanism and effect of SPM media on TEM data is critical for the application of TEM method to these targets.

There have been extensive studies of MV effect on TEM data. Lee [24] derived the analytical solution of MV effect based on the Chikazumi model. Kozhevnikov and Antonov [10], [25] gave the numerical formulas of MV effect over a layered-earth for the fixed loop and coincided loop source configuration. Sattel and Mutton [26] presented the results of MV effect for the airborne TEM survey, based on the modules of Maxwell package. Macnae [27] compared the MV effect of the land-based and airborne TEM configuration and summarized their regulations and differences. However, all these researches are based on conventional loop source TEM configuration, little has been conducted to the grounded-wire source configuration except that Antonov and Kozhevnikov [28] derived the formula for calculating the effect of magnetic relaxation on the horizontal electric field and cooresponding apparet resistivity. Compared with the loop source TEM method, the grounded-wire source TEM configuration is considered to have a larger detecting depth by using a high power source. The recently developed MTEM and SOTEM configurations have made the grounded-wire source TEM method widely used in mineral and hydrocarbon exploration [29], [30]. Therefore, the study of MV effect on grounded-wire source TEM method is important to guarantee the accuracy of the inversion of the data when SPM medium is presented.

In this paper, we focused on the MV effect on grounded-wire source TEM method. We first derive the formula for calculating the response due to the MV effect based on the Chikazumi model. Then, we analyze the dependence of MV effects on the resistivity, susceptibility, offset and the geometry of the SPM layer. Finally, we utilize the relative error due to MV effect to quantify the MV effect and obtain a solution to suppress the MV effect in a TEM survey. The results in the paper can be used as a guide for the installation of fieldwork of grounded-wire TEM survey.

II. BASIC THEORY

A. MAGNETIC SUSCEPTIBILITY FROM CHIKAZUMI MODEL

The method for calculating the TEM response over the medium with magnetic viscosity effect is based on magnetic susceptibility from Chikazumi model, a mathematical model to describe the hysteresis characteristics of SPM grains [31]. The model assumes that the magnetic moments of ferromagnetic particles decay logarithmically, and has been verified by rock physical experiments and field cases [12], [14], [16]. In Chikazumi Model, the magnetization J of the SPM medium, when withdrawing a constant magnetic field H_0 at t = 0, can be described as:

$$J(t) = J_0 \frac{1}{\ln(\tau_2/\tau_1)} \times \left(\int_{t/\tau_2}^{+\infty} \frac{\exp(-y)}{y} dy - \int_{t/\tau_1}^{+\infty} \frac{\exp(-y)}{y} dy \right), \quad (1)$$

where τ_1 and τ_2 are the lower and upper constants of the relaxation time respectively. Following Lee [32] and Kozhevnikov and Antonov [33], it is assumed that $\tau_1 = 10^{-6}$ and $\tau_2 = 10^6$ in this paper. J_0, which is the initial magnetization of the medium, is related to the magnetic field as $J_{0=}\chi_s H_0$, where χ_s is the time-independent static susceptibility. The time-dependent susceptibility can be expressed as follows through dividing both sides of equation (A1) by the static magnetic field H_0:

$$\chi(t) = \chi_s \frac{1}{\ln(\tau_2/\tau_1)} \int_{t/\tau_2}^{t/\tau_1} \frac{\exp(-y)}{y} dy. \quad (2)$$

Equation (2) can be simplified by replacing its integral argument y with t/τ:

$$\chi(t) = \chi_s \frac{1}{\ln(\tau_2/\tau_1)} \int_{\tau_1}^{\tau_2} \frac{\exp(-t/\tau)}{\tau} d\tau, \quad (3)$$

where t denotes the observation time and $\tau_1 \ll t \ll \tau_2$. We can get the frequency-dependent magnetic susceptibility from equation (2) using Fourier transform

$$\chi(\omega) = \chi_s \left[1 - \frac{1}{\ln(\tau_2/\tau_1)} \ln\left(\frac{1 + i\omega\tau_2}{1 + i\omega\tau_1} \right) \right] \quad (4)$$

where ω is the angular frequency.

B. FORWARD MODELING OF TEM RESPONSE OVER SPM MEDIUM

In this section, we present two algorithms for calculating the TEM responses over SPM medium. For comparative purpose, we first derive the formulas of a homogeneous SPM half-space using the time-dependent susceptibility, based on the research of Kozhevnikov and Antonov [33] and assumption that the eddy current and MV effect are two separated processes. Then we give the recursive equations for the SPM layered earth by solving the frequency domain Helmholtz equation with the frequency-dependent susceptibility. The digital filtering technique is used to transform the frequency domain response to the time domain.

1) HOMOGENEOUS SPM HALF-SPACE

The formulas for calculating the responses over a homogeneous SPM half-space are derived directly in the time domain. Thus, the method is referred as the time-domain solution in the follow-up discussions. The magnetic induction intensity

induced on a nonmagnetic half-space by a grounded wire source with current I_0 is

$$B_1 = I_0 LSM_0, \tag{5}$$

where L is the length of the grounded wire, S is the effective area of the sensor, M_0 is the coefficient of inductance between the transmitter and the loop on nonmagnetic earth. When a superparamagnetic object existing in the earth, the induced magnetic induction intensity is

$$B_2 = I_0 LSM_0 \chi_e, \tag{6}$$

where χ_e is the effective time-varying susceptibility that is related to $\chi(t)$, the shape of the magnetic object, and the type of source we adopted. For uniform magnetic half-space, the effective time-varying susceptibility is [34]:

$$\chi_e(t) = \left[\frac{\mu_1 - \mu_0}{\mu_1 + \mu_0} - 1\right] \chi(t) \tag{7}$$

where μ_0 and μ_1 are the magnetic permeability of the free space and half-space, respectively.

The magnetic permeability and susceptibility can be related as:

$$\mu = 1 + \chi \tag{8}$$

Substituting (8) into (7), the effective time-varying susceptibility becomes:

$$\chi_e(t) = \frac{2}{2 + \chi_s} \chi(t) \tag{9}$$

For most condition, $\chi_s \ll 1$, and $\chi_e(t) = \chi(t)$.

The total magnetic induction intensity induced in the receiver can be obtained by superposing B_1 and B_2:

$$B = B_1 + B_2 = I_0 LSM_0 [1 + \chi_e(t)]. \tag{10}$$

We define the inductance that incorporates the effect of the superparamagnetic objects and the nonmagnetic earth the effective inductance M_e,

$$M_e(t) = [1 + \chi_e(t)] M_0. \tag{11}$$

so that the secondary magnetic induction intensity induced in the receiver can be written with Duhamel's integral:

$$B(t) = I(t) M_0 LS + LS \int_{-\infty}^{t} I(\tau) \frac{dM_e(t-\tau)}{dt} d\tau. \tag{12}$$

By incorporating the step-off source waveform and taking derivatives of both side of equations with respect to time, the induced voltage in the receiver can be obtained:

$$\dot{B}(t) = -\delta(t) I_0 LSM_0 - I_0 LSM_e(t), \tag{13}$$

where $\delta(t)$ is the Dirac delta function. The first term in equation (13) is the response due to the eddy current effect of nonmagnetic earth while the second term is the response due to the MV effect of the superparamagnetic object. Substituting (10) into the second term of (13), the response due to the MV effect can be presented as:

$$\dot{B}_z^M(t) = -\frac{1}{\ln(\tau_2/\tau_1)} \frac{I_0 LS \chi_s \mu_0}{4\pi r^2 t} \sin\varphi. \tag{14}$$

The detailed derivations are listed in the appendix.

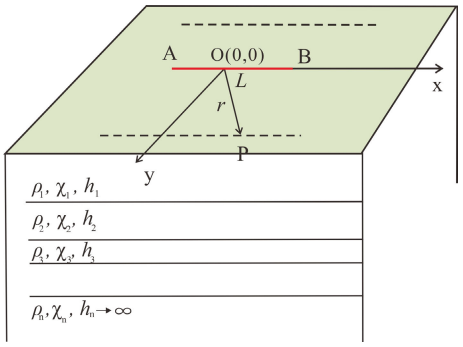

FIGURE 1. The schematic of the TEM measurement over a SPM layered earth. The red line is the grounded wire source and P in the dashed line represent the recording station.

2) SPM LAYERED EARTH

In the next step, we consider a layered magnetic model, as is shown in Fig. 1. Each layer can be characterized by a vector that includes the resistivity ρ, susceptibility χ and thickness h. The permeability of the air layer is set as the susceptibility μ_0 in a vacuum. The grounded-wire source is deployed at the surface of the earth with a length of L and current of I_0. The derivation of the response over SPM layered earth is performed in the frequency domain, thus the method is referred as frequency-domain solution in the follow-up discussions.

The response of the system in Fig. 1 can be calculated in the frequency domain recursively. We incorporate the frequency-dependent susceptibility to the frequency-domain vertical magnetic field and obtain [35]:

$$B_z(\omega) = \frac{\mu_0 I_0 [1 + \chi_i(\omega)]}{4\pi} \times \int_{-L/2}^{L/2} \frac{y}{r} \int_0^{\infty} (1 + r_{TE}) e^{u_0 z} \frac{\lambda^2}{u_0} J_1(\lambda r) d\lambda, \tag{15}$$

where

$$\chi_i(\omega) = \chi_{is} \left[1 - \frac{1}{\ln(\tau_2/\tau_1)} \ln\left(\frac{1 + i\omega\tau_2}{1 + i\omega\tau_1}\right)\right]$$

is the frequency-dependent magnetic susceptibility of layer i, and

$$u_i^2 = k_i^2 + \lambda_i^2 \tag{16}$$

$$k_i^2 = i\omega\mu_0 [1 + \chi_i(\omega)] / \rho_i - \omega^2 \mu_0 [1 + \chi_i(\omega)] \varepsilon_i \tag{17}$$

is wavenumber, J_1 is the first-order Bessel function.

r_{TE} is the reflection coefficient of the layered-earth:

$$r_{TE} = \frac{Y_0 - \hat{Y}_1}{Y_0 + \hat{Y}_1} \tag{18}$$

in which

$$Y_0 = \frac{u_0}{i\omega\mu_0} \tag{19}$$

and the recursive formula of $\hat{Y}_1$ is:

$$\hat{Y}_i = Y_i \frac{\hat{Y}_{i+1} + Y_i \tanh(u_i h_i)}{Y_i + \hat{Y}_{i+1} \tanh(u_i h_i)} \tag{20}$$

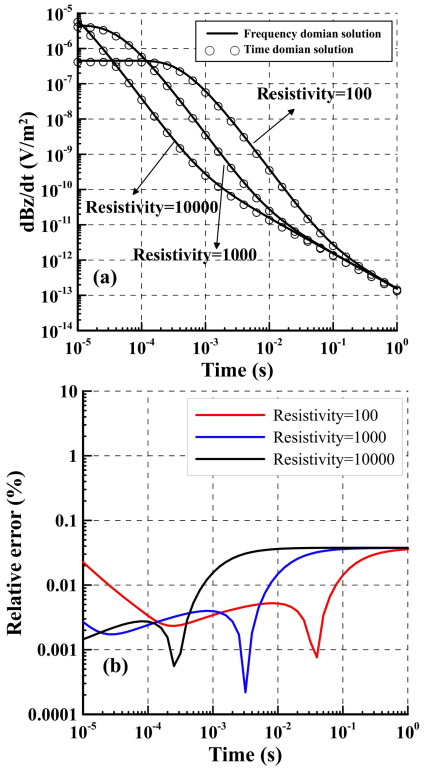

FIGURE 2. The comparison of the responses from the time domain solution and frequency solution. (a) the decay curves; (b) the relative error.

Since the thickness of Nth layer is infinite

$$\hat{Y}_N = Y_N = \frac{u_N}{i\omega\left[1+\chi\left(\omega\right)\right]\mu_0} \tag{21}$$

The time-domain response can be obtained with a digital filtering method of Cosine transform:

$$B_z(t) = -\frac{2}{\pi}\int_0^\infty \mathrm{Re}\left[H_z(\omega)\right]\cos\omega t d\omega. \tag{22}$$

3) NUMERICAL VALIDATION

To validate the derived formulas for calculating the TEM response over SPM medium, we compare the responses from the two methods above. The length of the grounded-wire source is 1000 m and the source current is 1 A. The center of the grounded-wire is set to (0 m, 0 m, 0 m) of the Cartesian coordinate. The recording station is located at (0 m, 500 m, 0 m). The relative magnetic susceptibility is 0.01 and the resistivity is set as $100\Omega\cdot m$, $1000\ \Omega\cdot m$ and $10000\Omega\cdot m$.

As is shown in Fig. 2a, the solutions from the time domain and frequency domain are in agreement with each other. We calculate the relative difference using the formula in equation (23) (Fig. 2b). The results demonstrate that the relative error is generally less than 5%. The consistency of the two methods illustrates the correctness of the proposed method.

$$\text{Relative error}=\frac{|M_t - M_b|}{M_b}, \tag{23}$$

TABLE 1. Parameters of the half-space model.

Model	Resistivity (ohm·m)	Susceptibility	Observation site
1	1000	0	(0,500)
2	1000	0.01	(0,500)
3	1000	0.1	(0,500)
4	100	0.01	(0,500)
5	10000	0.01	(0,500)
6	1000	0.01	(0,100)
7	1000	0.01	(0,1000)

where M_t and M_b represent the response over magnetic and nonmagnetic half-space respectively.

III. DEPENDENCE OF MV EFFECTS ON MODEL PARAMETERS

In this section, we analyze how the MV effect varies with the resistivity, susceptibility, geometry of the earth. The analysis is based on the formulas derived in the previous section. We design seven models to examine these dependencies and the parameters of the model are shown in TABLE 1. In the forward calculation, the length of the grounded wire is 1000 m and the current is 1A.

A. RESISTIVITY AND SUSCEPTIBILITY

Fig. 3a compares the responses from the models with different susceptibility using the designed model 1, 2 and 3. The decay curves coincide with each other at the early time and the departure with each other at late time. The time of the departure varies with the susceptibility. The larger the susceptibility is, the earlier the departure will take place. On the other hand, for the SPM models with the same susceptibility and different resistivity (model 2, 4 and 5), the decay curves departure with each other at early time, while coinciding with each other at the late time (Fig. 3b). When the medium is more resistive, the coincident point will be at an earlier time.

The features of decay curves in Fig. 3 reveal the intrinsic mechanism of the MV effect. Excited by the direct current in the grounded-wire source, the superparamagnetic grains will be magnetized to the direction of the primary field. When the source is switched off at $t = 0$, the effect of MV and eddy current will generate two types of secondary field. The eddy current will induce a secondary field $\dot{B}_z^E$ and the magnetization relaxation will generate a secondary filed $\dot{B}_z^M$, which form the total field after the source is turned off. Both $\dot{B}_z^E$ and $\dot{B}_z^M$ are in the same direction of the primary magnetic field.

If the resistivity of the model is high enough and the susceptibility is low enough (e.g. the relative susceptibility is higher than 0.1 or the resistivity is higher than $1\ \Omega\cdot m$), the eddy current effect and MV effect can be assumed to be independent [33], [36]. The inductive secondary field over a

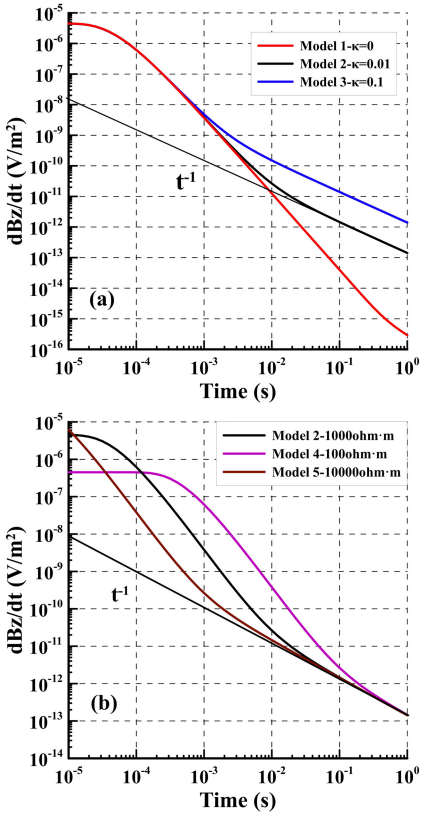

FIGURE 3. The decay curves from different models in Table 1. (a) from models with the same resistivity and different susceptibility; (b) from models with the same susceptibility and different resistivity.

homogeneous half-space is

$$B_z^E(t) = \frac{\mu_0 I_0 L}{4\pi r^2}\left[1-\left(1-\frac{3}{u^3}\right)\Phi(u)-\sqrt{\frac{2}{\pi}}\left(\frac{3}{u}\right)e^{-u^2/2}\right]\sin\varphi, \tag{24}$$

where $u = 2\pi r/\sqrt{2\pi\rho t\cdot 10^7}$, $\Phi(u)$ is the probability integral function. The variance of the susceptibility in Fig. 3a has little effect on the decay curve at the early time. We conclude that the response due to eddy current is much larger than that of the MV effect. Thus, the eddy current dominates the total field at the early time. For the late time, the inductive secondary field in equation (24) can be approximated as

$$\dot{B}_z^E(t) \approx= -\frac{IL\mu_0^{5/2}}{40\pi^{3/2}}\cdot\rho_1^{-3/2}\cdot t^{-5/2}\cdot r\cdot\sin\varphi. \tag{25}$$

Equation (25) reveals that the decay rate of $\dot{B}_z^E(t)$ is $t^{-5/2}$, while that of $\dot{B}_z^M(t)$ is t^{-1}, as is shown in (14). As the total field at the late time can be obtained by adding up $\dot{B}_z^E(t)$ and $\dot{B}_z^M$, the secondary field resulting from the MV effect dominates at the late time, which is consistent to the modeling result in Fig. 3b.

B. OFFSET

Fig.4 shows the decay curves from different source-receiver separation (offset) using model 6, 2 and 7 in Table 1.

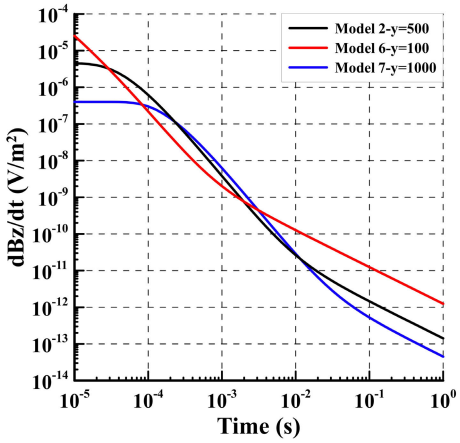

FIGURE 4. The decay curves from models with a different offset in Table 1.

The decay rate of curves change at different time for the responses from different offsets. The larger the offset is, the latter the changes occur. As is pointed out in the previous section, the changes of decay rate is due to the dominance of MV effect at late time. Therefore, we simulated the horizontal distribution of $B_z^E(t)$ and $B_z^M(t)$ for model 2 in Table 1, as is shown in Fig. 5 and Fig. 6. The grounded-wire source is located at (x =0m, y =0m) of the coordinate in the figure along the direction of x-axis. The length of the grounded-wire source is 1000 m and the source current is 1 A.

The slices of the time derivatives of the magnetic field at the earth surface indicate that the maximum of $\dot{B}_z^E(t)$ migrates away from the source, while the maximum of $\dot{B}_z^M(t)$ remains at the source position. The migration is caused by the horizontal diffusion of the eddy current over time. As both of the secondary fields attenuate rapidly with time, the migration of the maximum inductive field with time will weaken the dominance of the MV effect at large offset. Thus, the MV effect in a field survey can be reduced by acquiring the data at a very large offset.

C. THE GEOMETRY OF SPM LAYER

Next, we discuss the relationship between the geometry of superparamagnetic layer and MV response. As is indicated in the previous section, the response due to MV effect dominate decays more slowly than that due to eddy current. $\dot{B}_z^M$ be begins to dominate the late-time response after the instant when $\dot{B}_z^M$ is equal to $\dot{B}_z^E$. Here, we refer to this instant as t_{Re} and use it as an indicator to evaluate the influence of MV effect on the TEM data.

We design a three-layer model and calculate the t_{Re} of decay curves with variable thickness of overburden and superparamagnetic layer. The parameters of the model are shown in Fig. 7 and the responses are calculated at an offset of 500 m. We disturb the thickness of the parameters D and H in Fig. 7 and plot t_{Re} in Fig. 8 in a D-H coordinate. D and H vary from 1 m to 1000 m. As is shown in the figure, the increase of the thickness of the SPM layer will

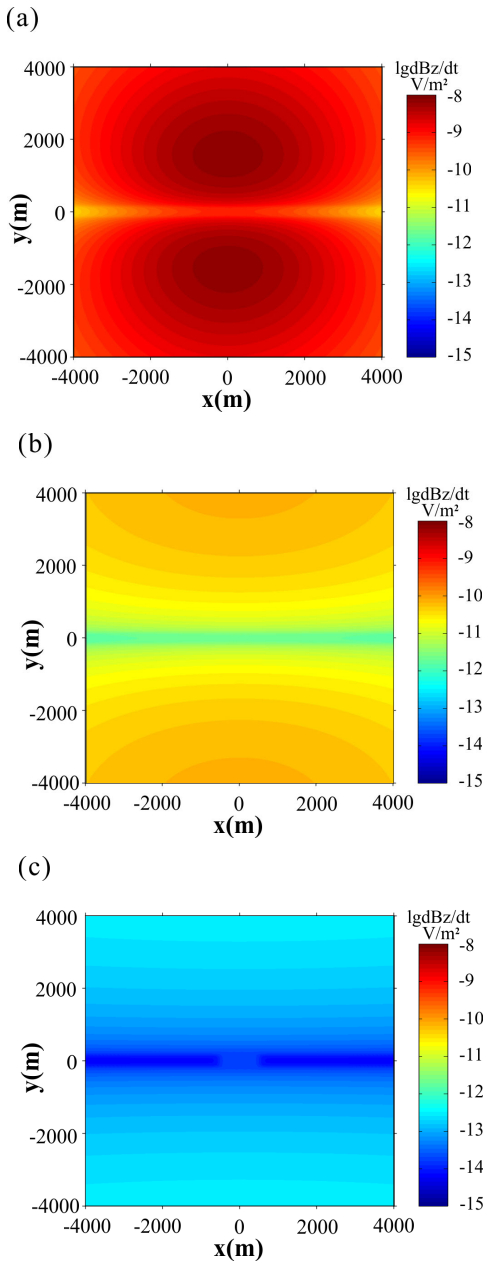

FIGURE 5. Horizontal distribution of the time derivatives of the magnetic field caused by eddy current at the earth surface. (a) 1ms; (b) 10ms; (c) 100ms.

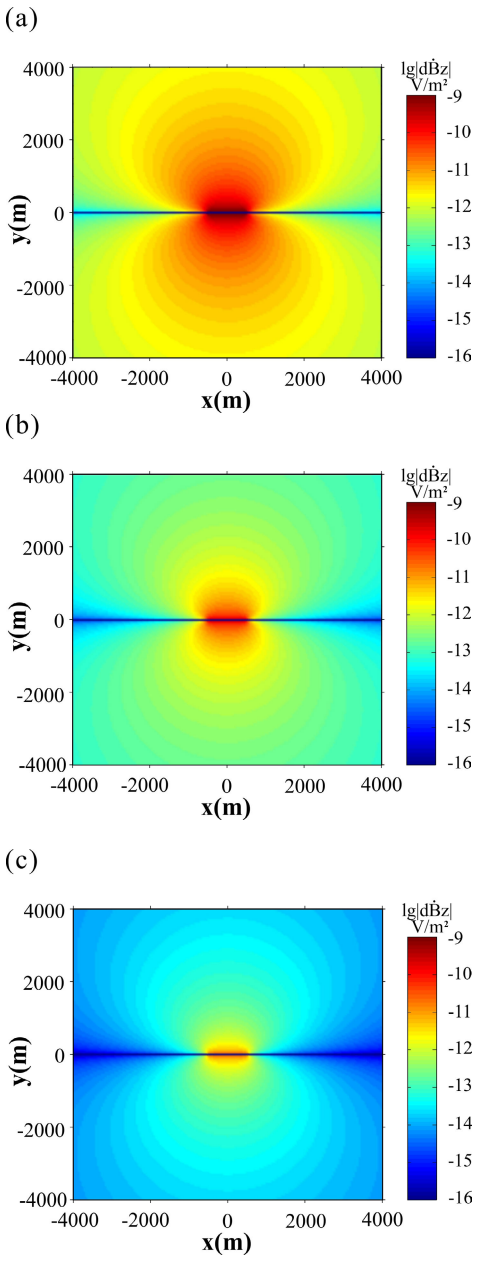

FIGURE 6. Horizontal distribution of the time derivatives of magnetic field caused by MV effect at the earth surface. (a) 1ms; (b) 10ms; (c) 100ms.

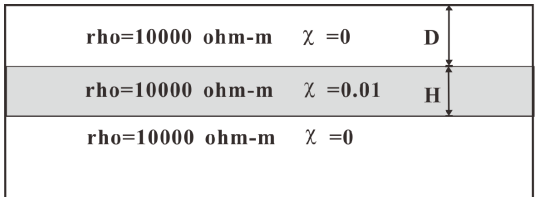

FIGURE 7. The model parameters of a three-layered model containing a SMP target layer.

monotonously bring forward the reversal of the sign. In addition, the reversal of sign will definitely occur even if the thickness of the SPM layer is small (e.g. 10 m). The t_{Re} can be ranged from 0.01 s to 1s, depending on the thickness of the overburden layer. Furthermore, t_{Re} will not monotonously decrease with the increase of the thickness of the overburden layer. Instead, t_{Re} will first increase and then decrease with the increase of the thickness of overburden layer.

The "counter-intuitive" reversal of t_{Re} in Fig. 8 can be revealed by analyzing the intrinsic mechanism of MV effect. In fact, this phenomenon was first revealed by Kozhevnikov and Antonov when they alaysised the MV response of inductive loop TEM [25]. They gave a convincing analysis of the this phenomenon with the concept of "demagnetization

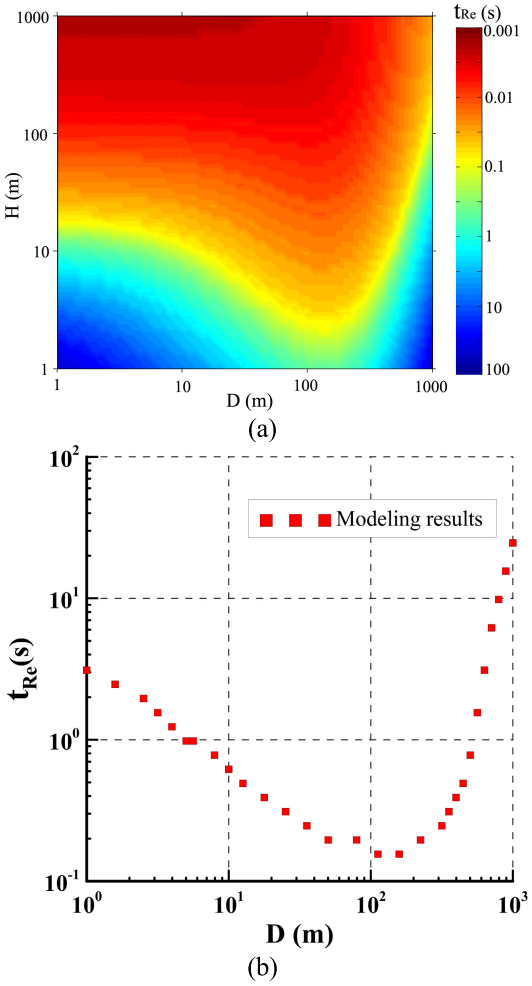

FIGURE 8. The t_{Re} for the models in Fig. 7 with different D and H. (a) Both D and H range from 1 m to 1000 m; (b)D ranges from 1 m to 1000 m and fix H=10, the red squares denote the sign reversal time of decay curves from different buried depth.

effects''. Considering a layered-earth containing two magnetic layers, the primary field generated by a horizontal grounded-wire source is presented by the red solid line in Fig. 9. Since the direction of the primary field in the magnetic layer 1and 2 are vertical and horizontal respectively, the direction of the magnetization of SPM grains shown in Fig.9b will be different. For the SPM grain 1 shown in Fig.9c, the direction of its magnetization is vertical so that the excited secondary field is opposite to the internal field of SPM grain 2. Thus, the total effective magnetization will be reduced. For SPM grain 3, the secondary field is parallel to the internal field of SPM grain 3. Thus, the total effective magnetization is strengthened. The phenomenon, in which the effective magnetization of magnetic object depends on its shape, is referred as shape demagnetization [37], [38]. Thus, the total effective magnetization of magnetic object can be written as $\boldsymbol{M} = \chi(1-\alpha)\boldsymbol{H}$, where α is the factor related to the shape of the magnetic object. For horizontal magnetic layer, $\alpha = 1/\alpha = 0$ when it is horizontally/vertically magnetized [39]. This is reason why the MV effect due to

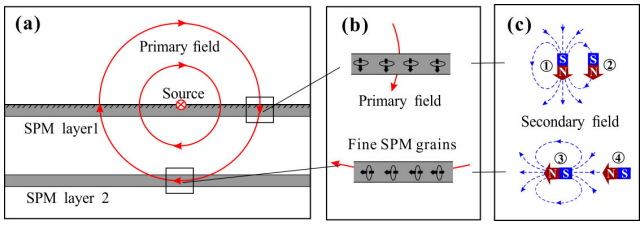

FIGURE 9. The magnetization and shape demagnetization mechanism The primary field in different layers; (b)The magnetization direction of fine SPM grains; (c) shape demagnetization.

a magnetic layer with certain buried depth is larger than that on the surface.

IV. QUANTIFICATION OF MV EFFECT ON TEM DATA

To suppress the MV effect in the TEM fieldwork, we quantitatively analyze the influence of MV effect on TEM observations through theoretical derivation and numerical simulation results. Based on the difference between non-magnetic half-space and magnetic half-space, the relative errors caused by the MV effect, which is calculated with equation (23), can be calculated as follows:

$$\text{Relative error}\,(t) = \left|\frac{\dot{B}_z^M(t)}{\dot{B}_z^E(t)}\right|. \tag{26}$$

Firstly, we quantify the relative error of the TEM response when a SPM layer is presented.Substituting equation (14) and (25) into (26), we have:

$$\lg[\text{Relative error}\,(t)] = \frac{3}{2}\lg t + \lg\chi_s - 3\lg r + \frac{3}{2}\lg\rho_1^{3/2} + C \tag{27}$$

where C can be calculated with:

$$C = \lg\left[\frac{5\pi^{1/2}}{\mu_0^{3/2}\ln(\tau_2/\tau_1)}\right].$$

To validate this quantification, we calculated the relative difference between the responses of Model 1 and 2 in Table 1, as is shown in Fig. 10. The relative error caused by MV effect increases exponentially with time. In the observation time ranging from 10^{-3} to10^{-1} s, the slope of the error curve can be approximated to $t^{1.5}$, which is consistent with (27).

In order to study the quantitative relationship between the relative error and the geo-electrical parameters as well as the offset parameter in (27), the time,t_{Re}, when $\dot{B}_z^M$ be begins to dominate the late-time response was analyzed. At the instant of t_{Re}, the secondary field caused by MV effect equals to the secondary field due to electromagnetic induction $B_z^M(t_r) = B_z^E(t_r)$, which makes the relative error at t_{Re} equal to 1.

The quantitative relationship between reversal time, susceptibility, resistivity and offset can be obtained:

$$\lg t_{\text{Re}} = 2\lg r - \frac{2}{3}\lg\chi_s - \lg\rho_1 + A \tag{28}$$

where $A = \lg\left[\frac{\ln(\tau_2/\tau_1)^{2/3}\mu_0}{5\pi^{1/3}}\right]$.

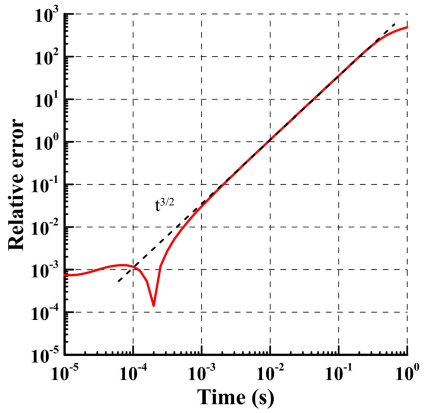

FIGURE 10. The calculated relative error between the responses of Model 1 and 2.

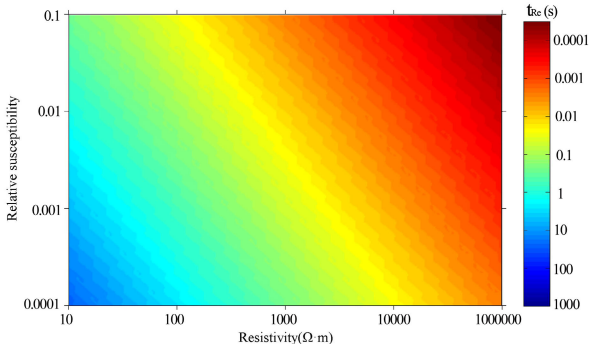

FIGURE 11. The variation of t_{Re} with respect to susceptibility and resistivity. The observing site is set at (0 m, 500 m, 0 m).

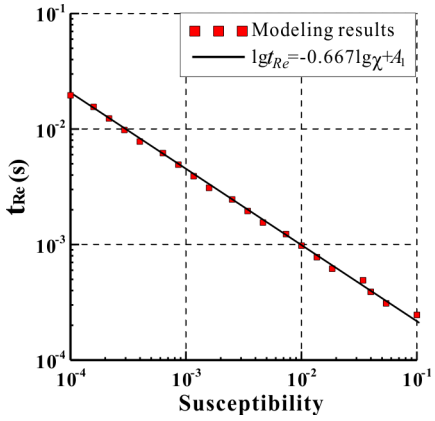

FIGURE 12. The t_{Re} for the model with different susceptibility. In the calculation, the offset is 500m while the resistivity of the model is 10000 Ω·m. A_1 is a constant related to A and the susceptibility of the model.

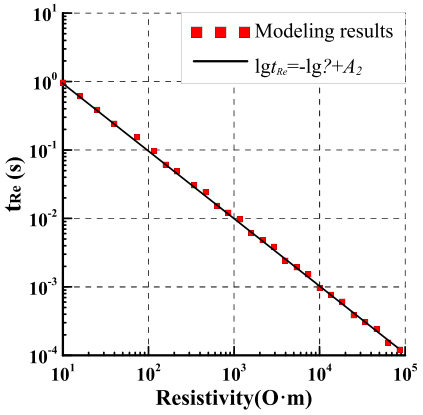

FIGURE 13. The t_{Re} for the model with different resistivity. In the calculation, the offset is 500m while the susceptibility of the model is 0.01. A_1 is a constant related to A and the resistivity of the model.

If the geo-electrical of survey area is known and t_{Re} can be estimated from observed data, an arbitrary relative error, such as 1% or 10%, due to MV effect can be estimated with (27) and (28). Thus, in next step, we validate equation (28) with numerical simulation. We disturb the resistivity and susceptibility of half-space model and plot the variation of t_{Re}, as is shown in Fig. 11. The resistivity varies from 10 to $10^5\Omega \cdot m$ while susceptibility is varied from 10^{-4} to 10^{-1}. The relationship between t_{Re} and resistivity, or t_{Re} and susceptibility can be extracted from Fig. 11, as is shown in Fig. 12 and 13. The slope of the t_{Re} - resistivity and t_{Re} -susceptibility curve can be approximated to $\chi^{-0.667}$ and ρ^{-1}, which is consistent with (28).

Next, we change the offset of the observing site. The sign reversal time (t_{Re}) of model 1 is shown in Fig. 14. The slope of the t_{Re}-offset curve can be approximated to r^2, which is consistent with the result of (26). It is worth noting that the modeling results deviate from the fitting curve when the offset is large. The deviation is due to the fact that equation (28) is derived based on the approximated solution in (25), which is only valid at near-field region or late time. Based on the numerical results in Fig.10-Fig.12, we have verified the validity of (28). For the half-space model, the influence of MV effect on TEM data depends on the offset and geo-electrical parameters of survey area.

As t_{Re} is closely related to the offset, we can adjust t_{Re} to be outside the time range of the TEM response by properly setting the offset when designing the survey. As is shown in Fig. 14, A_3 is a constant that depends on geo-electrical parameter of the earth. If a prior field experiment or petrophysical results are available, t_{Re} can be estimated and the MV effect can be dramatically suppressed by recording the TEM data at the offset range where the influence of MV effect is beyond the time range of the response. One thing should be noted when estimate the susceptibility is that, according to the work of James, SPM mainly results from single domain particles while the bigger particles add to static susceptibility [18].

However, the magnetic half-space model is only suitable for region covered with thick tuff layer. Driven by the weathering denudation, water erosion, ancient cultural activities and the enrichment of magnetotactic bacteria, these SPM grains usually gather on the surface and form a magnetic

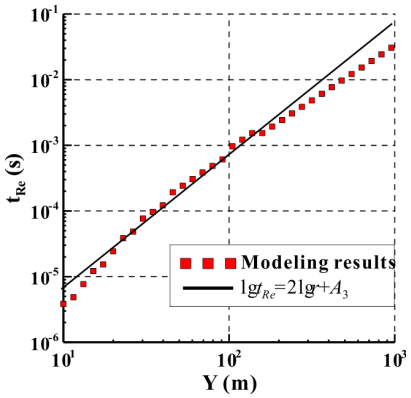

FIGURE 14. The t_{Re} of magnetic half-space earth, model 2. In the calculation, the offset varies from 10 to 10^3 m.A_3 is a constant related to A and the geo-electrical parameters of the model.

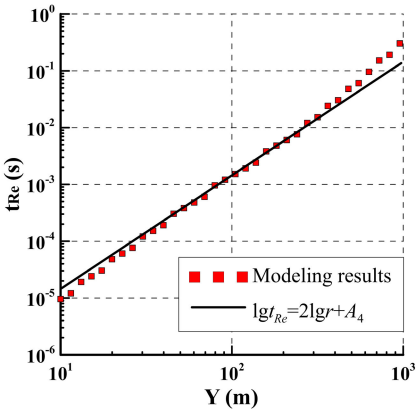

FIGURE 15. The t_{Re} of magnetic two-layered earth. The thickness of the first layer is 100 m. The resistivity of the model is 1000 Ω·m, the susceptibility of layer 1 and 2 are 0.01 and 0 respectively while the offset of observing site varying from 10 to 10^3m.

layer. Thus, a magnetic layered-model is more practical for actual geological conditions. Given that the SPM grains mainly originate from shallow magmatic rocks, such as basalt and tuff, we consider the relationship between t_{Re} and offset for the magnetic two-layered model as is shown in Fig. 15. The thickness of the first layer is 100 m, the resistivity of the model is 1000 Ω·m, the susceptibility of the two layers are 0.01 and 0 respectively while the offset of observing site varying from 10 to 10^3m. It is indicated that the slope of the t_{Re}-offset curve can also be approximated to r^2, which verifies that the conclusions that we draw from half-space model are still valid for the layered model.

V. A CASE HISTORY IN BAYAN OBO DEPOSIT

In this section, we present a case history in Bayan Obo deposit and then analysis the MV effect with pratical TEM data. The method we proposed for suppressing the MV effect with an optimal offset will also be tested.

A. GEOLOGICAL SETTING OF BAYAN OBO REGION

The Bayan Obo deposit is an important iron deposit in China, and also the largest rare earth element (REE) accumulation

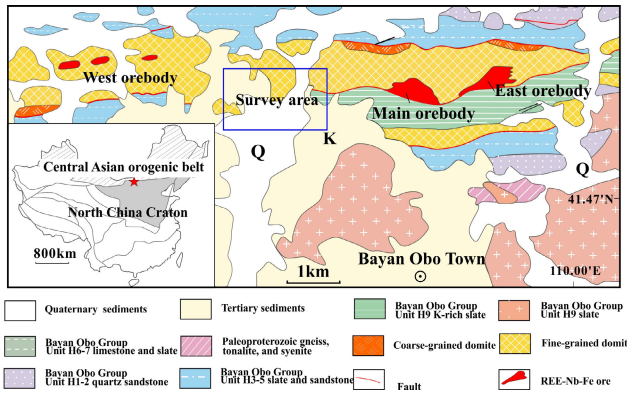

FIGURE 16. Geological map of Bayan Obo (China) rare deposit.(modified from [42]).

in the world. It is located in approximately 150 km north of Baotou, Inner Mongolia province, China [40]. On the regional scale, the Bayan Obo region lies in the northern margin of the North China craton (Figure 16). The strata exposed in the mining area mainly include Mesoproterozoic Bayan Obo Group and Archean Paleoproterozoic basement rocks. The basement is mianly consists of migmatized gneiss, quartz schist, amphibolite anorthosite and granulite while the Bayan Obo Group is a suite of low-grade metamorphic rocks consisting of dolomite, quartzite, slate and carbonatite and was divided into18 units (H1–H18) [41]. All the iron orebodies,including east, west, and main orebodies, occur in the dolomite that can be classified as H8 unit. The main iron minerals are magnetite and hematite, most of which are in the form of fine-grained block. The other minerals include fluorite, aegirine, tremolite, biotite, dolomite, apatite, pyrite, monazite, bastnaesite, etc.

B. GROUNDED-WIRE TEM SURVEY

From October to November,2019, we carried out a grounded-wire TEM survey in Bayan Obo deposit. The purpose of the survey was to prospect the geo-electrical structure of Bayan Obo region and provided geophysical information for estimating the REE and iron reserves.

The instrument used for this project was the V8 system developed by Phoenix Geophysics and a magnetic sensor (SB-7K) with effective receiving areas of 40,000m^2. A bipolar current (duty cycle is 50%) with base frequency of 2.5 Hz was injected to excite the EM field. Corresponding to the base frequency, the TEM data at the timescale between 1 and 100 ms were observed.

This project included 11 survey lines with length ranging from 1km to 8km. We found that the ∂Bz/∂t decay curves observed in the segment AB of survey line 1 and the segment CD in survey line 2 (in Figure 17) exhibited a negative slope with an approximate t^{-1} time dependence. It should be noted that AB was located at a tailing hill that has been piled up for several decades and CD was near the ore deposit. The offset for survey line 1 and 2 are approximately 270m and 380m,

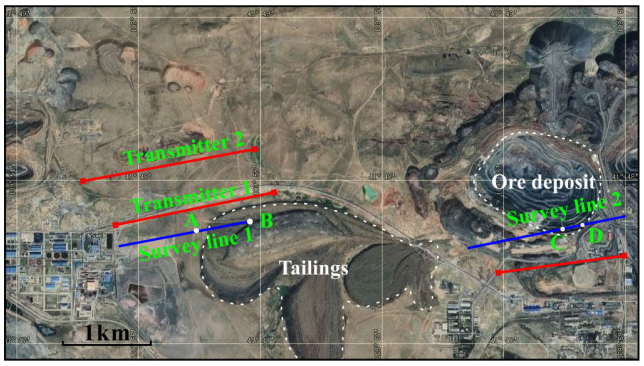

FIGURE 17. Layout of the transmitters and survey lines.

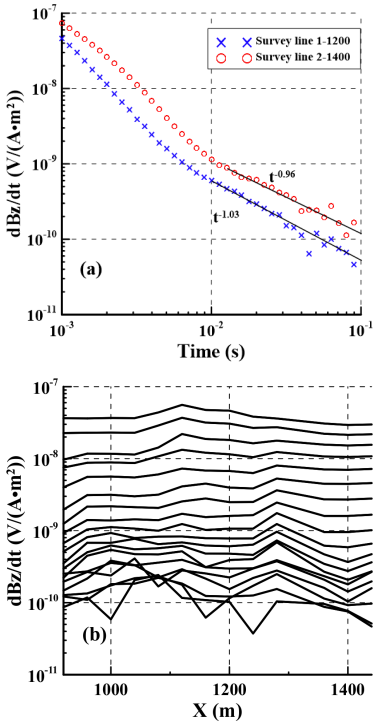

FIGURE 18. The observed TEM data that with an approximate t^{-1} time dependence (a) The decay curves at site 1200 of survey line 1 and site 1400 of survey line 2. (b)The multi-chanel curves of sites from 920 (site A) to 1440 (site B).

respectively. According to the previous modeling results of this paper, these decay curves were similar to MV response whose late-time decays rate is also t^{-1} in log-log coordinate system.

In next step, we identify the MV effect in the observed TEM data with two methods. One is to study the susceptibility of the rock and ore in Bayan Obo deposite. Wang et al.(2016) measured 1146 hand samples from the orebody, host rock and tailing with proton magnetometer (G856AX) [43]. A Part of his result are listed in TABLE 2. According to statistics, the average susceptibility of metamorphic basement, host rock, basite and minerals are approximately $4600*10^{-5}$SI, $600*10^{-5}$SI, $3500*10^{-5}$SI, $28000*10^{-5}$SI, respectively. The other is to use the scanning electron microscope to confirme fine-grained magnetic grains. As shown in Figure 19, the backscattered electron image of tailing sample confirm the existence of fine hematite amd pyrite grains. With these two methods and the late-time decays rate, it is believed that the anomaly observed in survey line 1 and 2 were result from MV effect.

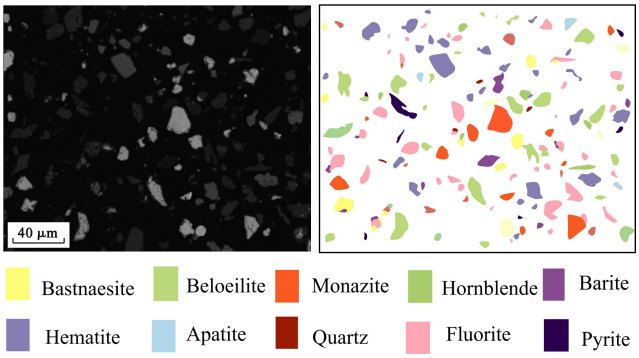

FIGURE 19. The backscattered electron image of tailing sample.

TABLE 2. The Susceptibility of the Rock and Ore samples in Bayan Obo deposit.

Rock	The Number of samples	Susceptibility/10^{-5}SI Max	Min	Average	Types
Gneiss	23	12824	1177	4656	Metamorphic basement
Slate	36	6546	218	1138	
Basalt	69	2398	739	1300	Basite
Andesite	341	3340	339	1010	
Gabbro diorite	19	14665	4989	8868	
Amphibolite	23	18225	356	3008	
Slate	26	1637	128	349	Host rock
Dolomite	38	4260	407	1425	
Carbonaceous slate	25	315	58	123	
Dolomitized magnetite	75	94206	71946	15000	Mineral
Hematite magnetite	30	192254	110538	155252	
Magnetite hematite	63	200960	9420	40506	
Limonite	13	1805	456	887	

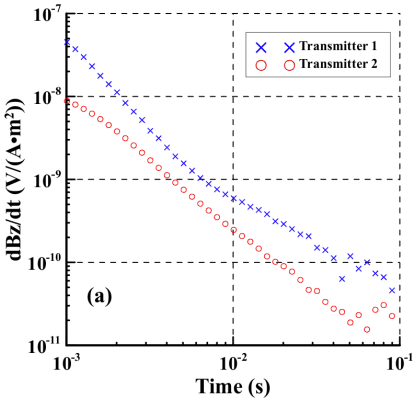

FIGURE 20. The responses due to different transmitters.

In order to to suppress the MV effect in the obsearved TEM data in survey line 1, we employed a new transmitter, namely, the transmitter 2 shown in Figure 17. The offset between transmitter 2 and survey line 1 is 790m. As shown in Figure 20, MV effect began to dominate the responses due to transmitter 1at about 10^{-2}s. And the MV response due to transmitter 2 was suppressed under the noise level. The inductive eddy effect dominated TEM response in the time scales between 1 to 50ms.

VI. CONCLUSION

We derive the formulas for calculating the secondary field of MV effect with a TEM citation. Thereafter, we examine the dependence of MV effect on model parameters. The MV effects are then quantified with the relative errors between the magnetic and nonmagnetic medium. The conclusions are as follows:

(A1) When the source is turned off, the eddy current and MV effect will be launched simultaneously. These two processes generate the secondary fields that are in the same direction. The inductive field caused by eddy current is dominant at the early time, while the secondary field due to the MV effect dominates the late time, which leads to a a slow decay rate of t^{-1} at late time.

(2) The MV effect mainly depends on the resistivity and susceptibility of the model. The higher the susceptibility or resistivity is, the earlier MV effect domain the total response.

(3) The influence of MV effect can be avoided by recording the TEM data at the proper offset range. When the estimates of the resistivity and permeability are available, the offset range can be calculated as use as a guide for the installation of grounded-wire TEM survey.

VII. DECLARATION OF INTEREST

The authors declare that there is no conflict of interests regarding the publication of this paper.

APPENDIX

In the appendix, we present the detailed derivation of the time solution of TEM response over SPM medium. The derivation is based on the secondary magnetic induction intensity induced by the constant current in the transmitter. When we use the source waveform $I(t)$ that turns off the current at $t = 0$

$$I(t) = I_0 [1 - \mathcal{H}(t)], \tag{A1}$$

where $\mathcal{H}(t)$ is the unit Heaviside function. Substituting (A1) into (12), we can get the magnetic field excited by a step-off source waveform:

$$\begin{aligned} B(t) &= I_0 LS [1 - \mathcal{H}(t)] M_0 \\ &+ I_0 LS \int_{-\infty}^{t} \frac{dM_e(t-\tau)}{dt} d\tau \\ &- I_0 LS \int_{-\infty}^{t} \mathcal{H}(t) \frac{dM_e(t-\tau)}{dt} d\tau. \end{aligned} \tag{A2}$$

The Integral with Heaviside function can be simplified as: $\int_{-\infty}^{t} H(t) \frac{dM_e(t-\tau)}{dt} d\tau = \int_{0}^{t} \frac{dM_e(t-\tau)}{dt} d\tau$. Thus, the integral in equation (A2) can be calculated explicitly:

$$\begin{aligned} B(t) &= [1 - \mathcal{H}(t)] I_0 LSM_0 \\ &+ I_0 LS [M_e(+\infty) - M_e(0)] - I_0 LS [M_e(t) - M_e(0)]. \end{aligned} \tag{A3}$$

As $\chi(t)$ decreases with the increase of time, $\chi(+\infty) = 0$. We have:

$$M_e(0) = [1 + \chi_e(0)] M_0. \tag{A4}$$

$$M_e(+\infty) = M_0. \tag{A5}$$

Substituting (A4) and (A5) to (A3):

$$B(t) = -\mathcal{H}(t) I_0 LSM_0 - I_0 LSM_e(t). \tag{A6}$$

In the next step, we take the derivative of both side of equation (A6) with respect to time and do some algebra, we obtain the time derivative of the magnetic field:

$$-\dot{B}(t) = \delta(t) I_0 LSM_0 + I_0 LS \frac{dM_e(t)}{dt}, \tag{A7}$$

where $\delta(t)$ is the Dirac delta function. The first term in (A7) is due to the eddy current of nonmagnetic earth, while the second term is due to the MV effect of the superparamagnetic object. Substituting equation (11) into the second term of (A7), the response due to the MV effect can be presented as:

$$\dot{B}_M(t) = I_0 LSM_0 \frac{d\chi_e(t)}{dt}. \tag{A8}$$

According to equation (3) and (7), the derivative of the effective susceptibility with respect to time is:

$$\frac{d\chi_e(t)}{dt} = \frac{\chi_s}{\ln(\tau_2/\tau_1)} \frac{1}{t} \left(e^{-t/\tau_2} - e^{-t/\tau_1}\right). \tag{A9}$$

Since $\tau_1 \ll t \ll \tau_2$, $e^{-t/\tau_2} \approx 1$ and e^{-t/τ_1} can be neglected, (A9) becomes:

$$\frac{d\chi_e(t)}{dt} = \frac{\chi_s}{\ln(\tau_2/\tau_1)} \frac{1}{t}. \tag{A10}$$

For a homogeneous nonmagnetic half-space earth, the primary static magnetic field due to a grounded-wire that energized by direct current is:

$$H_0 = -\frac{I_0 LS}{4\pi r^2} \sin\varphi. \tag{A11}$$

in which r is the distance between the midpoint of the wire and the receiver and $\sin\varphi = y \Big/ \sqrt{x^2 + y^2}$.

$$M_0 = -\frac{\mu_0}{4\pi r^2} \sin\varphi. \tag{A12}$$

Substituting (A10)~(A12) to (A8), the response due to MV effect can be obtained:

$$\dot{B}_z^M(t) = -\frac{1}{\ln(\tau_2/\tau_1)} \frac{I_0 LS \chi_s \mu_0}{4\pi r^2 t} \sin\varphi. \tag{A13}$$

REFERENCES

[1] G. Xue, S. Yan, L.-J. Gelius, W. Chen, N. Zhou, and H. Li, "Discovery of a major coal deposit in china with the use of a modified CSAMT method," *J. Environ. Eng. Geophys.*, vol. 20, no. 1, pp. 47–56, Mar. 2015.

[2] M. Birsan, "A Bayesian approach to electromagnetic sounding in a marine environment," *IEEE Trans. Geosci. Remote Sens.*, vol. 41, no. 6, pp. 1455–1460, Jun. 2003.

[3] A. V. Christiansen, E. Auken, and A. Viezzoli, "Quantification of modeling errors in airborne TEM caused by inaccurate system description," *Geophysics*, vol. 76, no. 1, pp. F43–F52, May 2014.

[4] A. Ziolkowski, B. A. Hobbs, and D. Wright, "Multitransient electromagnetic demonstration survey in France," *Geophysics*, vol. 72, no. 4, pp. F197–F209, Jul. 2007.

[5] S. Krivochieva and M. Chouteau, "Whole-space modeling of a layered earth in time-domain electromagnetic measurements," *J. Appl. Geophys.*, vol. 50, no. 4, pp. 375–391, Jul. 2002.

[6] G. Buselli, "The effect of near-surface superparamagnetic material on electromagnetic measurements," *Geophysics*, vol. 47, no. 9, pp. 1315–1324, Sep. 1982.

[7] C. Colani and M. J. Aitken, "Utilization of magnetic viscosity effects in soils for archaeological prospection," *Nature*, vol. 212, no. 5069, pp. 1446–1447, Dec. 1966.

[8] P. Barsukov and E. Fainberg, "Superparamagnetic effect over gold and nickel deposits," *Eur. J. Environ. Eng. Geophys.*, vol. 72, no. 6, pp. 61–72, 2001.

[9] M. Montonen, "SPM effect in glacial till," *ASEG Extended Abstr.*, vol. 2015, no. 1, pp. 1–4, Dec. 2015.

[10] N. Kozhevnikov and E. Antonov, "The magnetic relaxation effect on TEM responses of a two-layer earth," *Russian Geol. Geophys.*, vol. 50, no. 10, pp. 895–904, Oct. 2009.

[11] D. C. Cowan, "Forward modeling and inversion of viscous remanent magnetization responsesin the time domain," Univ. British Columbia, Vancouver, BC, Canada, 2016.

[12] V. Stognii, N. Kozhevnikov, and E. Antonov, "TEM surveys for magnetic viscosity of rocks in situ," *Russian Geol. Geophys.*, vol. 51, no. 11, pp. 1219–1226, Nov. 2010.

[13] F. E. S. Gaucher and R. S. Smith, "The impact of magnetic viscosity on time-domain electromagnetic data from iron oxide minerals embedded in rocks at Opemiska, Québec, Canada," *Geophysics*, vol. 82, no. 5, pp. B165–B176, Sep. 2017.

[14] L. R. Pasion, S. D. Billings, and D. W. Oldenburg, "Evaluating the effects of magnetic soils on TEM measurements for UXO detection," in *Proc. SEG Int. Exposit. 72nd Annu. Meeting*, 2002, pp. 2–5.

[15] N. Bournas, "Superparamagnetic effects discrimination in VTEM data of Greenland using multiple criteria and predictive approaches," *J. Appl. Geophys.*, vol. 145, pp. 59–73, Oct. 2017.

[16] M. Dabas and J. R. Skinner, "Time-domain magnetization of soils (VRM), experimental relationship to quadrature susceptibility," *Geophysics*, vol. 58, no. 3, pp. 326–333, 2002.

[17] K. Pisane, E. Despeaux, and M. Seehra, "Magnetic relaxation and correlating effective magnetic moment with particle size distribution in maghemite nanoparticles," *J. Magn. Magn. Mater.*, vol. 384, pp. 148–154, Jun. 2015.

[18] J. Macnae, "Definitive superparamagnetic source identification through spatial, temporal, and amplitude analysis of airborne electromagnetic data," *Geophys. Prospecting*, vol. 65, no. 4, pp. 1071–1084, Jul. 2017.

[19] J. Macnae, "Quantitative estimation of intrinsic induced polarization and superparamagnetic parameters from airborne electromagnetic data," *Geophysics*, vol. 81, no. 6, pp. E433–E446, Nov. 2016.

[20] T. Chen, H. Xu, Q. Xie, J. Chen, J. Ji, and H. Lu, "Characteristics and genesis of maghemite in Chinese loess and paleosols: Mechanism for magnetic susceptibility enhancement in paleosols," *Earth Planetary Sci. Lett.*, vol. 240, nos. 3–4, pp. 790–802, Dec. 2005.

[21] N. O. Kozhevnikov, A. V. Kharinsky, and O. K. Kozhevnikov, "An accidental geophysical discovery of an iron age archaeological site on the western shore of lake baikal," *J. Appl. Geophys.*, vol. 47, no. 2, pp. 107–122, Jun. 2001.

[22] J. Igel, H. Preetz, and S. Altfelder, "Magnetic viscosity of tropical soils: Classification and prediction as an aid for landmine detection," *Geophys. J. Int.*, vol. 190, no. 2, pp. 843–855, Aug. 2012.

[23] T. Kratzer, J. Macnae, and P. Mutton, "Detection and correction of SPM effects in airborne EM surveys," *Explor. Geophys.*, vol. 44, no. 1, pp. 6–15, Mar. 2013.

[24] T. Lee, "The transient electromagnetic response of a magnetic or superparamagnetic ground," *Geophysics*, vol. 49, no. 7, pp. 854–860, Jul. 1984.

[25] N. Kozhevnikov and E. Antonov, "Magnetic relaxation of a horizontal layer: Effect on TEM data," *Russian Geol. Geophys.*, vol. 52, no. 4, pp. 398–404, Apr. 2011.

[26] D. Sattel and P. Mutton, "Modelling the superparamagnetic response of AEM data," *Explor. Geophys.*, vol. 46, no. 1, pp. 118–129, Mar. 2015.

[27] J. Macnae, "Superparamagnetism in ground and airborne electromagnetics: Geometrical and physical controls," *Geophysics*, vol. 82, no. 6, pp. E347–E356, Nov. 2017.

[28] E. Y. Antonov and N. O. Kozhevnikov, "Magnetic viscosity effect on 'grounded-line transient responses of a uniform conducting earth,'" *Russian Geol. Geophys.*, vol. 58, pp. 857–865, 2017.

[29] W. Chen, "A comparison of loop time-domain electromagnetic and short-offset transient electromagnetic methods for mapping water-enriched zones—A case history in Shaanxi, China," *Geophysics*, vol. 82, no. 6, pp. B201–B208, 2017.

[30] N. Zhou, D. Hou, and G. Xue, "Effects of shadow and source overprint on grounded–wire transient electromagnetic response," *IEEE Geosci. Remote Sens. Lett.*, vol. 15, no. 8, pp. 1169–1173, Aug. 2018.

[31] S. H. Chickazumi and S. Charap, *Physics of Magnetism*. New York, NY, USA: Huntington, 1978.

[32] T. Lee, "The effect of a superparamagnetic layer," *Geophys. Prospecting*, vol. 32, pp. 480–496, Mar. 1984.

[33] N. Kozhevnikov and E. Antonov, "The magnetic relaxation effect on TEM responses of a uniform earth," *Russian Geol. Geophys.*, vol. 49, no. 3, pp. 197–205, Mar. 2008.

[34] G. V. Keller and F. C. Frischknecht, *Electrical Methods in Geophysical Prospecting*. London, U.K.: Pergamon Press, 1966.

[35] M. N. Nabighian, *Electromagnetic Methods in Applied Geophysics*. Tulsa, OK, USA: Society of Exploration Geophysicists, 1991.

[36] W. Guo, M. C. Dentith, R. T. Bird, and D. A. Clark, "Systematic error analysis of demagnetization and implications for magnetic interpretation," *Geophysics*, vol. 66, no. 2, pp. 562–570, Mar. 2001.

[37] M. B. J. Purss and J. P. Cull, "A new iterative method for computing the magnetic field at high magnetic susceptibilities," *Geophysics*, vol. 70, no. 5, pp. L53–L62, Sep. 2005.

[38] W. Williams and D. J. Dunlop, "Three-dimensional micromagnetic modelling of ferromagnetic domain structure," *Nature*, vol. 337, no. 6208, pp. 634–637, Feb. 1989.

[39] G. J. Borradaile and M. Jackson, "Structural geology, petrofabrics and magnetic fabrics (AMS, AARM, AIRM)," *J. Struct. Geol.*, vol. 32, no. 10, pp. 1519–1551, 2010.

[40] M. P. Smith, L. S. Campbell, and J. Kynicky, "A review of the genesis of the world class Bayan Obo Fe–REE–Nb deposits, Inner Mongolia, China: Multistage processes and outstanding questions," *Ore Geol. Rev.*, vol. 64, pp. 459–476, Jan. 2015.

[41] K. Yang, H. Fan, M. Santosh, F. Hu, and K. Wang, "Mesoproterozoic carbonatitic magmatism in the Bayan Obo deposit, Inner Mongolia, North China: Constraints for the mechanism of super accumulation of rare earth elements," *Ore Geol. Rev.*, vol. 40, pp. 122–131, Sep. 2011.

[42] K. Yang, H. Fan, F. Pirajno, and X. Li, "The Bayan Obo (China) giant REE accumulation conundrum elucidated by intense magmatic differentiation of carbonatite," *Geology*, vol. 47, no. 12, pp. 1198–1202, Dec. 2019.

[43] W. Jichun, S. Chongyu, and W. Zhili, "A comprehensive comparative study of geological characteristics as well as aeromagnetic and aeroradiometric features of the Bayan Obo REE-Nb-Fe depoits and their implications for prospecting work," *Geol. China*, vol. 43, no. 2, pp. 594–606, 2016.

LINBO ZHANG received the B.S. degree in geophysics from the China University of Mining and Technology, Xuzhou, China, in 2016. He is currently pursuing the Ph.D. degree in geophysics with the Institute of Geology and Geophysics (subordinate to the Institutions of Earth Science of the Chinese Academy of Sciences), University of the Chinese Academy of Sciences. His research interests include the analytic solutions of Earth-ionosphere mode controlled source electromagnetic method, the numerical modeling of the TEM response of short-offset excited by grounded electric sources, and the correction of additional effect in TEM data.

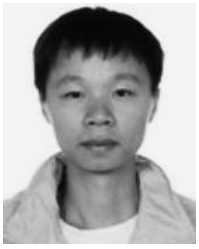

HAI LI received the bachelor's degree from Central South University, in 2011, and the Ph.D. degree from the University of Chinese Academy of Sciences, in 2016. He is currently a Postdoctoral Fellow with the Key Laboratory of Mineral Resources, Institute of Geology and Geophysics (subordinate to the Innovation Academy for Earth Science of the Chinese Academy of Sciences). His research interests include the data processing and imaging of TEM data, the inversion method for CSEM method, the induced polarization effect on TEM data, and the case history of CSEM method. He is currently a member of SEG and EAGE.

GUOQIANG XUE is currently a Researcher with the Key Laboratory of Mineral Resources, Institute of Geology and Geophysics (subordinate to the Innovation Academy for Earth Science of the Chinese Academy of Sciences), and also a Professor with the College of Earth and Planetary Sciences, University of the Chinese Academy of Sciences, with an emphasis in transient electromagnetic exploration and applications. His research interests include TEM pseudo-seismic interpretation method, TEM tunnel predication studies, large loop TEM exploration technology, the TEM response of short-offset excited by grounded electric sources, and analysis of time-varying point charge infinitesimal assumptions in the TEM field. He is also an Associate Editor of the JEEG and the *Applied Geophysics*.

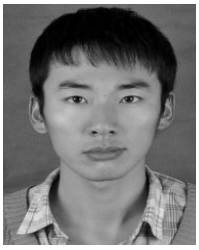

WEN CHEN is born in Heilongjiang, China, in 1993. He received the bachelor's degree in geophysics from Jilin University, Changchun, China, in 2012. He is currently pursuing the Ph.D. degree with the Key Laboratory of Mineral Resources, Institute of Geology and Geophysics (subordinate to the Innovation Academy for Earth Science of the Chinese Academy of Sciences). His current research focuses on three-dimensional forward modeling of time-domain electromagnetic method with IP effect and extraction of IP information from measured electromagnetic data.

YIMING HE was born in Liaoning, China, in 1995. He received the bachelor's degree from the China University of Mining and Technology, Xuzhou, in 2017. He is currently pursuing the Ph.D. degree with the Institute of Geology and Geophysics (subordinate to the Institutions of Earth Science of the Chinese Academy of Sciences), University of the Chinese Academy of Sciences. His research topic is the data processing of airborne and semi-airborne TEM data.